SCIENTIFIC REPORTS

OPEN

Received: 22 June 2015
Accepted: 16 September 2015
Published: 21 October 2015

Luminescent Iridium(III) Complexes Supported by N-Heterocyclic Carbene-based C^C^C-Pincer Ligands and Aromatic Diimines

Lai-Hon Chung[1], Hoi-Shing Lo[1,2], Sze-Wing Ng[1], Dik-Lung Ma[3], Chung-Hang Leung[4] & Chun-Yuen Wong[1,2]

Iridium(III) hydrido complexes containing N-heterocyclic carbene (NHC)-based pincer ligand 1,3-bis(1-butylimidazolin-2-ylidene)phenyl anion (C^1^C^C^1) or 1,3-bis(3-butylbenzimidazolin-2-ylidene) phenyl anion (C^2^C^C^2) and aromatic diimine (2,2′-bipyridine (bpy), 1,10-phenanthroline (phen), 4,4′-dimethyl-2,2′-bipyridine (Me_2bpy), or dipyrido-[3,2-f:2′,3′-h]-quinoxaline (dpq)) in the form of $[Ir(C^C^C)(N^N)(H)]^+$ have been prepared. Crystal structures for these complexes show that the Ir–C_{NHC} distances are 2.043(5)–2.056(5) Å. The hydride chemical shifts for complexes bearing C^1^C^C^1 (−20.6 to −20.3 ppm) are more upfield than those with C^2^C^C^2 (−19.5 and −19.2 ppm), revealing that C^1^C^C^1 is a better electron donor than C^2^C^C^2. Spectroscopic comparisons and time-dependent density functional theory (TD-DFT) calculations suggest that the lowest-energy electronic transition associated with these complexes ($\lambda = 340$–530 nm ($\varepsilon \leq 10^3$ dm^3 mol^{-1} cm^{-1})) originate from a $d_\pi(Ir^{III}) \rightarrow \pi^*(N^N)$ metal-to-ligand charge transfer transition, where the $d_\pi(Ir^{III})$ level contain significant contribution from the C^C^C ligands. All these complexes are emissive in the yellow-spectral region (553–604 nm in CH_3CN and CH_2Cl_2) upon photo-excitation with quantum yields of 10^{-3}–10^{-1}.

Polypyridyl ruthenium(II) or other d^6-transition metal complexes represent an important class of emissive molecular material[1–14]. Their triplet $[d_\pi(M) \rightarrow \pi^*(\text{polypyridyl})]$ metal-to-ligand charge transfer (^{3}MLCT) excited-states are known to derive rich photophysical and photochemical properties, and their applications in solar energy conversion[11,15], organic light emitting devices (OLEDs)[16], photochemistry[11,12], and bio-labelling reagents[17] have received considerable interest. Regarding the design of transition metal-containing luminophores, iridium(III) center has received great attention on the basis that it is a heavier analogue of ruthenium(II) center[18,19].

After the isolation of stable NHCs by Arduengo and co-workers in 1991[20], intensive investigations on NHCs and the derived metal complexes have been centralized on the development of catalytic reagents for organic transformations[21–25]. On the other hand, employment of N-heterocyclic carbenes (NHCs)-derived ligands as an alternative of polypyridines in the design of transition metal-based luminophores is growing to be an important research topic recently. For example, emissive Ru(II)[26], Ir(III)[18,19], and Pt(II)[27] complexes supported by NHCs have been reported. Several emissive NHC-containing

[1]Department of Biology and Chemistry, City University of Hong Kong, Tat Chee Avenue, Kowloon, Hong Kong SAR. [2]State Key Laboratory of Millimeter Waves, City University of Hong Kong, Tat Chee Avenue, Kowloon, Hong Kong SAR. [3]Department of Chemistry, Hong Kong Baptist University, Kowloon Tong, Hong Kong SAR. [4]State Key Laboratory of Quality Research in Chinese Medicine, Institute of Chinese Medical Sciences, University of Macau, Macao, China. Correspondence and requests for materials should be addressed to C.-Y.W. (email: acywong@cityu.edu.hk)

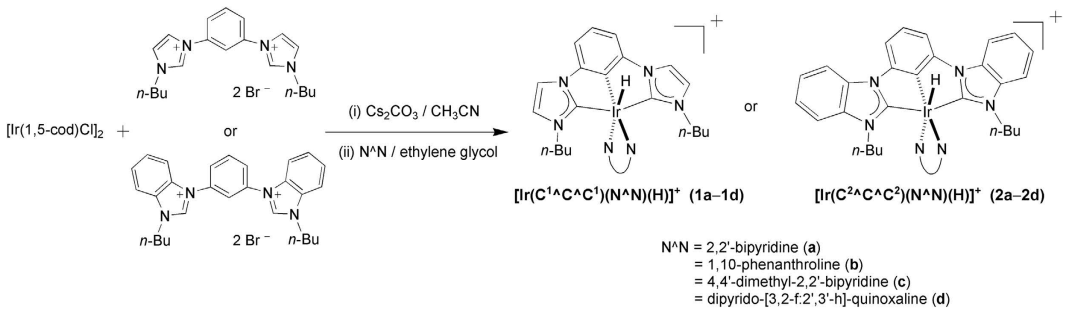

Figure 1. Synthetic route of 1–2

multinuclear Cu, Ag, and Au complexes have also been prepared, in which the NHCs facilitate the metal-metal interaction-induced emissions[28,29].

We have initiated a program to develop organometallic Ru(II)/Os(II)–diimine and related luminophores[30–33], and very recently we have reported emissive osmium(II) carbonyl complexes bearing 1,3-bis(1-methylimidazolin-2-ylidene)phenyl anion ($^{Me}C^1\text{^}C\text{^}C^{1Me}$) or 1,3-bis(3-m ethylbenzimidazolin-2-ylidene)phenyl anion ($^{Me}C^2\text{^}C\text{^}C^{2Me}$) and aromatic diimine in the form of $[Os(C\text{^}C\text{^}C)(N\text{^}N)(CO)]^+$ [30]. Spectroscopic and theoretical investigations on $[Os(C\text{^}C\text{^}C)(N\text{^}N)(CO)]^+$ have revealed that the emissive state for $[Os(C\text{^}C\text{^}C)(N\text{^}N)(CO)]^+$ originates from a $d_\pi(Os^{II}) \rightarrow \pi^*(N\text{^}N)$ MLCT transition, where the C^C^C ligands contribute significantly to both the $d_\pi(Os^{II})$ and $\pi^*(N\text{^}N)$ levels. This suggests that the NHC-derived ligands would not only act as point charge/spectator ligands, but can also be involved in the emissive excited-state to modify the photophysical properties of a metal–diimine luminophore. As an extension to scrutinize the effect of C^C^C pincer ligands on the photophysical properties of a [M(N^N)] moiety, we now present the preparation, spectroelectrochemical, photophysical, and theoretical investigations of a class of emissive hydrido iridium(III) complexes bearing C^C^C pincer ligands and aromatic diimines, $[Ir(C\text{^}C\text{^}C)(N\text{^}N)(H)]^+$.

Results

Synthesis. Emissive Ir(III) complexes $[Ir(C\text{^}C\text{^}C)(N\text{^}N)(H)]^+$ (**1**–**2**) were prepared by refluxing $[Ir(C\text{^}C\text{^}C)(CH_3CN)(Br)(H)]$ with N^N in ethylene glycol (Figure 1). $[Ir(C\text{^}C\text{^}C)(CH_3CN)(Br)(H)]$ were synthesized analogously to the corresponding known complexes $[Ir(^{Ar}C\text{^}C\text{^}C^{Ar})(CH_3CN)(Cl)(H)]$ and $[Ir(^{Me}C^1\text{^}C\text{^}C^{1Me})(CH_3CN)(I)(H)]$ ($^{Ar}C\text{^}C\text{^}C^{Ar}$ = 1,3-bis(1-arylimidazolin-2-ylidene)phenyl anion)[23,24]. The presence of the hydride ligands in **1**–**2** was confirmed by the ^{1}H NMR signals at −20.6 to −19.2 ppm and ν_{Ir-H} at 2126 to 2189 cm^{-1}. Both the ^{1}H and ^{13}C NMR spectra signify that **1**–**2** possess a pseudo-plane of symmetry in solution on the NMR time scale at room temperature. For instances, there are 17 and 19 sets of aromatic ^{13}C signal for **1a** and **1b**, respectively. The ^{13}C NMR signals at 167.8–180.6 ppm for **1**–**2** are typical for metalated NHC. It is noted that the hydride chemical shifts for **1a**–**1d** (−20.55 to −20.27 ppm) are nearly 1 ppm more upfield than those for **2a**–**2d** (−19.50 to −19.21 ppm). Since the hydride chemical shifts indicate that the electronic shielding effect of the hydrido group results from the metal core's electron cloud, they can be used as probes for the donating ability of the C^C^C ligands[34]. Therefore, the more upfield hydride chemical shifts for **1a**–**1d** when compared with **2a**–**2d** reveals that $C^1\text{^}C\text{^}C^1$ is a stronger electron donor than $C^2\text{^}C\text{^}C^2$. The same conclusion has recently been made in the comparison of the ν_{CO} between $[Os(^{Me}C^1\text{^}C\text{^}C^{1Me})(N\text{^}N)(CO)]^+$ and $[Os(^{Me}C^2\text{^}C\text{^}C^{2Me})(N\text{^}N)(CO)]^+$ [31]. These findings are also consistent with the NHC donor strengths determined by Huynh *et al.*, where benzimidazolin-2-ylidene is suggested to have a weaker donor strength compared with imidazolin-2-ylidene[35]. Complex $[Ir(C^1\text{^}C\text{^}C^1)_2]^+$ has also been synthesized according to the method reported in literature[23] for spectroscopic comparisons.

The molecular structures of **1a**(ClO_4), **2a**(ClO_4), and [**2b**(ClO_4)]$_3$·CH_3CN have been determined by X-ray crystallography. Perspective views of the cations **1a** and **2b** are depicted in Figure 2; selected bond distances and angles are summarized in Table 1. In each case, the Ir atom adopts a distorted octahedral geometry, with the C^C^C-pincer coordinating in a meridional mode. The ring systems on C^C^C are not perfectly co-planar: the NHC moieties (i.e. imidazolin-2-ylidene or benzimidazolin-2-ylidene units) are tilted towards the hydride ligands, and the angles between the NHC planes are 12.36–22.54°. These angles are larger than those found in $[Ir(^{Me}C^1\text{^}C\text{^}C^{1Me})(CH_3CN)(I)(H)]$, $[Ir(C\text{^}^{Me}C^{Me}\text{^}C)(CH_3CN)(I)_2]$ ($C\text{^}^{Me}C^{Me}\text{^}C$ = 1,3-bis(1-butylimidazolium)-4,6-dimethylbenzene) and $[Ir(^{Ar}C\text{^}C\text{^}C^{Ar})(CH_3CN)(Cl)(H)]$ in which the angles between the NHC planes are 2.73°, 3.63° and 5.60–15.58° respectively[23,24]. As a comparison, the ring systems on C^C^C for $[Os(^{Me}C^1\text{^}C\text{^}C^{1Me})(N\text{^}N)(CO)]^+$ and $[Os(^{Me}C^2\text{^}C\text{^}C^{2Me})(N\text{^}N)(CO)]^+$ (N^N = bpy or phen) are more close to a co-planar configuration (angles between the NHC planes are 2.30–13.00°)[31]. The C_{NHC}–Ir–C_{Ph} angles for these complexes are 77.22(11)–78.74(15)°, which are only slightly larger than the C_{NHC}–Os–C_{Ph} angles in $[Os(^{Me}C^1\text{^}C\text{^}C^{1Me})(N\text{^}N)(CO)]^+$ and $[Os(^{Me}C^2\text{^}C\text{^}C^{2Me})(N\text{^}N)(CO)]^+$ (75.6(3)–76.8(3)°)[31]. The Ir–C_{NHC} distances (2.043(5)–2.056(5) Å) are notably longer than the Ir–C_{Ph} distances (1.959(4)–1.986(5) Å). Similar findings have been observed

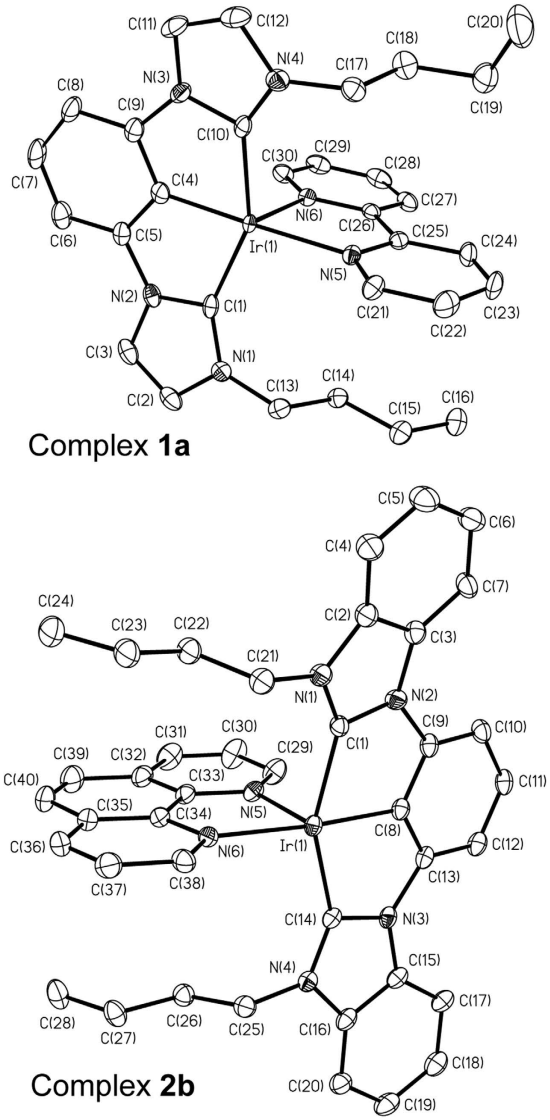

Figure 2. Perspective views of **1a** (top) and **2b** (bottom); thermal ellipsoids are at the 50% and 30% probability level, respectively. Hydrogen atoms are omitted for clarity.

complex	1a	2a	2b
Ir–C_{NHC}	2.049(3), 2.055(3)	2.044(4), 2.046(4)	[2.052(5), 2.056(5)]; [2.045(5), 2.049(5)]; [2.043(5), 2.044(5)]
Ir–C_{Ph}	1.975(3)	1.959(4)	1.986(5); 1.982(5); 1.980(5)
Ir–$N_{N^\wedge N}$ (trans to Ph)	2.130(2)	2.134(3)	2.140(4); 2.134(4); 2.149(4)
Ir–$N_{N^\wedge N}$ (trans to H)	2.144(2)	2.154(3)	2.135(5); 2.148(4); 2.141(5),
C_{NHC}–Ir–C_{Ph}	77.22(11), 77.86(11)	78.30(15), 78.74(15)	[77.7(2), 77.8(2)]; [77.8(2), 77.9(2)]; [77.7(2), 78.7(2)]
∠Ph/NHC	7.90, 16.96	5.06, 7.35	[4.86, 10.71]; [8.21, 8.35]; [3.35, 10.50]
∠NHC/NHC	22.54	12.36	14.83; 16.41; 13.85

Table 1. Selected Bond Lengths (Å) and Angles (deg) for 1a, 2a, and 2b. The angle between the rings (∠Ph/NHC or ∠NHC/NHC) are calculated from all non-hydrogen atoms on the ring moiety). For **2b**, the crystal contains three crystallographically independent Ir complexes in an asymmetric unit; structural data from each complex are grouped in brackets and listed in the order of Ir(1), Ir(2), and Ir(3).

Complex	$E_{1/2}$/V vs $Cp_2Fe^{+/0}$	
	reduction	oxidation
1a	−1.93	$E_{pa} = 0.7$
1b	−1.95	$E_{pa} = 0.71$
1c	−2.00	$E_{pa} = 0.69$
1d	−1.83	$E_{pa} = 0.70$
2a	−1.87	$E_{pa} = 0.76$
2b	−1.87	$E_{pa} = 0.76$
2c	−1.95	$E_{pa} = 0.73$
2d	−1.73	$E_{pa} = 0.77$
$Ir(C^1\text{^}C\text{^}C^1)_2]^+$	—	0.71

Table 2. Electrochemical Data. Supporting electrolyte: 0.1 M $[Bu_4N]PF_6$ in CH_3CN. $E_{1/2} = (E_{pc} + E_{pa})/2$ at 298 K for reversible couples. Anodic peak potential (E_{pa}) at scan rate of 100 mV s^{-1} are recorded for irreversible oxidation wave.

in $[Ir(^{Me}C^1\text{^}C\text{^}C^{1Me})(CH_3CN)(I)_2]$[23], $[Ir(^{Me}C^1\text{^}C\text{^}C^{1Me})(CH_3CN)(I)(H)]$[24], $[Ir(C\text{^}^{Me}C^{Me}\text{^}C)(CH_3CN)(I)_2]$ ($C\text{^}^{Me}C^{Me}\text{^}C$ = 1,3-bis(1-butylimidazolium)-4,6-dimethylbenzene)[23], $[Ir(^{Ar}C\text{^}C\text{^}C^{Ar})(CH_3CN)(Cl)(H)]$[24], and Zr, Rh, and Os complexes bearing similar C^C^C-pincer ligands[31,36]. Since the Ir–C_{Ph} distances in *fac*-$[Ir(C\text{^}C)_3]$ and *mer*-$[Ir(C\text{^}C)_3]$ (C^C = 1-phenyl-3-methylbenzimidazolin-2-ylidene-*C*,*C*$^{2'}$) are in the range of 2.071(7)−2.099(4) Å[18], the significantly shorter Ir–C_{Ph} distances in this work most likely arise from the strain intrinsic to the metal–C^C^C moieties.

Electrochemistry. Cyclic voltammetry has been used to examine the electrochemistry of the complexes (Table 2; all values vs $Cp_2Fe^{+/0}$). **1**–**2** show irreversible first oxidation waves at $E_{pa} = 0.69$ to 0.77 V (scan rate = 100 mV s^{-1}), and reversible first reduction couples at $E_{1/2} = -2.00$ to −1.73 V. It is noted that both the first oxidation waves and the first reduction couples are sensitive to the change of C^C^C and N^N. For example, the first reduction potentials for **1a**–**1d** (−2.00 to −1.83 V) are slightly more negative than those for **2a**–**2d** (−1.95 to −1.73 V), and the ease of reduction follows the order: **d** > **b** ≈ **a** > **c**. These findings suggest that both the highest occupied molecular orbitals (HOMOs) and the lowest unoccupied molecule orbitals (LUMOs) for **1**–**2** contain contributions from the C^C^C and N^N, in agreement with our DFT calculations (see discussion below). Moreover, the contribution of N^N to the LUMOs of **1**–**2** is apparent as $[Ir(C^1\text{^}C\text{^}C^1)_2]^+$ does not feature any reduction wave within the solvent window.

UV–Visible Absorption and Spectroelectrochemistry. The UV–visible spectral data for **1**, **2**, and $[Ir(C^1\text{^}C\text{^}C^1)_2]^+$ are summarized in Table 3, and their absorption spectra are depicted in Figure 3. **1**–**2** exhibit intense, high-energy absorptions at $\lambda \leq 340$ nm ($\varepsilon \geq 10^4$ dm^3 mol^{-1} cm^{-1}), and moderately intense bands at $\lambda > 340$ nm ($\varepsilon \approx 10^3$ dm^3 mol^{-1} cm^{-1}) with tailing up to 530 nm. In the literature, Ir(III) complexes bearing aromatic diimine ligands such as $[Ir(bpy)_3]^{3+}$ and $[Ir(phen)_3]^{3+}$ feature highly intense absorptions at $\lambda \leq 320$ nm ($\varepsilon \geq 10^4$ dm^3 mol^{-1} cm^{-1}), and these are ascribed to $\pi \rightarrow \pi^*$(N^N) intraligand (IL) transitions[37–39]. In addition, $[Ir(C^1\text{^}C\text{^}C^1)_2]^+$ exhibits intense absorptions at $\lambda \leq 330$ nm ($\varepsilon \geq 10^4$ dm^3 mol^{-1} cm^{-1}), which are expected to be a mixture of $d_\pi(Ir^{III}) \rightarrow \pi^*$(C^C^C) metal-to-ligand charge transfer (MLCT) and $\pi \rightarrow \pi^*$(C^C^C) IL transition. With the origin of absorptions for $[Ir(N\text{^}N)_3]^{3+}$ and $[Ir(C^1\text{^}C\text{^}C^1)_2]^+$ as references, the high-energy absorptions at $\lambda \leq 340$ nm for complexes **1**–**2** are assigned to be a mixing of $\pi \rightarrow \pi^*$(C^C^C) IL, $\pi \rightarrow \pi^*$(N^N) IL, and $d_\pi(Ir^{III}) \rightarrow \pi^*$(C^C^C) MLCT transitions.

On the other hand, the electronic transitions at $\lambda = 340$–530 nm ($\varepsilon \leq 10^3$ dm^3 mol^{-1} cm^{-1}) for **1**–**2** should contain some $d_\pi(Ir^{III}) \rightarrow \pi^*$(N^N) MLCT character, reasons are as follows: (1) $[Ir(bpy)_3]^{3+}$, $[Ir(phen)_3]^{3+}$, and $[Ir(ppy)_2(bpy)]^+$ (ppy = 2-phenylpyridine) feature $d_\pi(Ir^{III}) \rightarrow \pi^*$(N^N) MLCT transitions in similar energy region ($\lambda_{max} = 370$–520 nm, $\varepsilon \leq 10^3$ dm^3 mol^{-1} cm^{-1});[38–43] (2) a red-shift in absorption energy is observed when N^N is changed from Me_2bpy to bpy, and from phen to dpq; (3) **1**–**2** display solvatochromic effect in the spectral region concerned. For example, the λ_{max} for **1a** within this spectral region is 374 nm in CH_3CN, and is 384 nm in CH_2Cl_2; (4) there are no corresponding absorption bands for $[Ir(C^1\text{^}C\text{^}C^1)_2]^+$. This assignment is consistent with the TD-DFT calculations on complexes **1a** and **2a**, which suggest that the nature of electronic transitions in the spectral region concerned to be mainly attributed to the HOMO−1 → LUMO and HOMO−2 → LUMO transitions, where the HOMO–1 and HOMO–2 have higher Ir contribution (27–59%) than that in LUMO (3–4%), and LUMO has higher N^N contribution (93%) than those in HOMO–1 and HOMO–2 (3–15%) (see discussion below). The contribution of N^N to the LUMOs for **1** and **2** is further confirmed by spectroelectrochemistry. Thin-layer UV–visible spectroelectrochemistry has been employed to acquire the absorption spectra for $\mathbf{1a}^-$ and $\mathbf{2a}^-$, the reduced forms of **1a** and **2a** respectively (Figure 4). The isosbestic spectral

complex	λ_{max}/nm (ε_{max}/dm^3 mol^{-1} cm^{-1})
Solvent = CH_3CN	
1a	241 (sh, 36670), 283 (26380), 308 (sh, 14980), 319 (sh, 11720), 374 (4240), 439 (sh, 1620)
1b	246 (33910), 260 (30980), 281 (sh, 21780), 308 (10680), 320 (11250), 370 (5460), 455 (sh, 1720)
1c	242 (sh, 37920), 281 (27830), 304 (sh, 16760), 321 (sh, 13090), 371 (4640), 430 (sh, 1950)
1d	250 (sh, 57990), 256 (58720), 288 (37050), 319 (14630), 374 (7180), 459 (sh, 2210)
2a	247 (63480), 271 (44590), 285 (sh, 35650), 309 (25000), 321 (22070), 370 (sh, 5240), 422 (sh, 1710)
2b	248 (57050), 269 (46670), 286 (sh, 30100), 312 (sh, 17530), 321 (19930), 376 (sh, 5090), 430 (sh, 1720)
2c	247 (64180), 270 (48540), 307 (26390), 322 (23220), 369 (sh, 5520), 425 (sh, 1650)
2d	248 (77070), 256 (74100), 285 (47240), 320 (23660), 365 (sh, 7060), 453 (sh, 1660)
$[Ir(C^1\text{^}C\text{^}C^1)_2]^+$	279 (18810), 305 (15410), 318 (15270)
Solvent = CH_2Cl_2	
1a	240 (sh, 40380), 285 (30500), 308 (sh, 15420), 318 (sh, 12550), 351 (4400), 384 (4510), 447 (sh, 1770)
1b	247 (sh, 34120), 262 (33960), 280 (sh, 22810), 309 (10810), 321 (11075), 375 (5690), 472 (sh, 1750)
1c	242 (sh, 40650), 283 (30940), 306 (sh, 16480), 322 (13600), 378 (4670), 422 (sh, 1980)
1d	252 (sh, 60080), 257 (61150), 289 (36820), 320 (14480), 381 (7310), 467 (sh, 2280)
2a	248 (67690), 272 (48350), 282 (sh, 45580), 309 (25340), 321 (23470), 375 (sh, 5460), 441 (sh, 1560)
2b	249 (65520), 269 (56000), 282 (sh, 40080), 311 (sh, 19100), 322 (22270), 385 (sh, 5890), 448 (sh, 1680)
2c	249 (63520), 272 (49670), 308 (25150), 323 (23440), 372 (sh, 5490), 431 (sh, 1820)
2d	249 (80990), 257 (76520), 286 (49670), 321 (23940), 379 (7330), 465 (sh, 1940)
$[Ir(C^1\text{^}C\text{^}C^1)_2]^+$	281 (19600), 305 (15680), 319 (15680)

Table 3. UV–Visible Absorption Data.

changes suggest that the electrochemical reductions of **1a** and **2a** are clean conversions. Notably, reductions of **1a** and **2a** result in enhancement of absorption at ~380 nm and new absorption doublet band near 500 nm. These absorption features were observed in the reduction of $[Ir(bpy)_3]^{3+}$ and are characteristic absorptions for anionic bpy radical ($bpy^{\bullet-}$)[44].

Emission Spectroscopy. The emission properties of the complexes in fluid solution (CH_3CN and CH_2Cl_2) at 298 K have been investigated (Table 4). Figure 5 depicts the emission spectra for **2a**, **2c**, **2d**, and $[Ir(C^1\text{^}C\text{^}C^1)_2]^+$ in CH_3CN at 298 K. Emission maxima of **1**–**2** range from 553 to 604 nm in CH_3CN and CH_2Cl_2 which are significantly blue shifted when compared with $[Os(C\text{^}C\text{^}C)(N\text{^}N)(CO)]^+$ (λ_{em} = 676–731 nm, solvents = CH_3CN and CH_2Cl_2)[30]. Quantum yields (Φ) and emission lifetimes (τ) of **1**–**2** are around 10^{-3}–10^{-1} and 10^2–10^1 ns respectively, while those parameters for $[Os(C\text{^}C\text{^}C)(N\text{^}N)(CO)]^+$ are around 10^{-4}–10^{-2} and 1–6 μs respectively[30]. Similar to $Os(C\text{^}C\text{^}C)(N\text{^}N)(CO)]^+$, these photophysical parameters for **1**–**2** are sensitive to the change of C^C^C and N^N, revealing that the emissive state involve both the C^C^C and N^N moieties. For example, in both **1**–**2** and $[Os(C\text{^}C\text{^}C)(N\text{^}N)(CO)]^+$, blue-shift on emission maxima, higher emission quantum yield, and longer excited state lifetime are observed when changing the N^N from 2,2-bipyridine to 1,10-phenanthroline[30]. The resemblance of the excitation profiles to the absorption spectra signifies that the emissions originate from the energy dissipation of the $d_\pi(Ir^{III}) \rightarrow \pi^*(N\text{^}N)$ MLCT transitions. Interestingly, similar conclusion has been made on the nature of the emissive excited states in $[Os(C\text{^}C\text{^}C)(N\text{^}N)(CO)]^+$ [30]. The emission profile for $[Ir(C^1\text{^}C\text{^}C^1)_2]^+$ is highly structured and the emission maxima (378 and 398 nm) are not sensitive to the change of solvent, therefore these emissions are assigned as $\pi \rightarrow \pi^*$ (C^C^C) ^{3}IL emissions.

Theoretical Calculations. Time-dependent density functional theory (TD-DFT) calculations have been performed on modeling complexes $[Ir(^{Me}C^1\text{^}C\text{^}C^{1Me})(bpy)(H)]^+$ (**1a'**) and $[Ir(^{Me}C^2\text{^}C\text{^}C^{2Me})(bpy)(H)]^+$ (**2a'**), in which their metal cores are the same as **1a** and **2a** but the butyl chains on the C^C^C are replaced by methyl groups to reduce computational cost. The ground-state structures of **1a'** and **2a'** have been optimized at the DFT level (functional = PBE0)[45,46] without symmetry constrain. The conductor-like screening model (COSMO)[47] has been applied to account for solvent effects upon the electronic transition. All the optimized geometries are in satisfactory agreement with their crystal structures. For example, the Ir–C_{NHC} and Ir–C_{Ph} bond distances calculated for **1a'** (2.05–2.06 and 1.97 Å respectively) are similar to those for **1a** determined by X-ray crystallography (Ir–C_{NHC}: 2.049(3) and 2.055(3) Å; Ir–C_{Ph}: 1.975(3) Å).

The excitation energies and oscillator strengths for the calculated vertical transitions with $\lambda > 360$ nm are summarized in Table 5. Table 6 summarized the compositions of the molecular orbitals (MOs) which

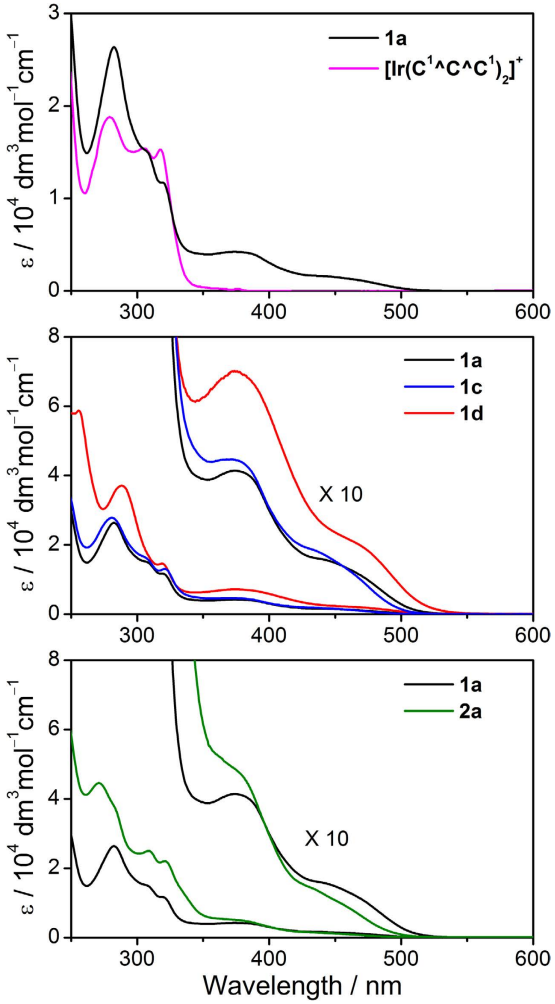

Figure 3. UV–visible absorption spectra of selected complexes in CH_3CN at 298 K.

are involved in the lowest-energy electronic transitions in these complexes. Figure 6 depicts the simulated absorption spectra. It is noted that the calculated lowest-energy dipole allowed transitions ($\lambda > 360$ nm) mainly originate from the HOMO–1 → LUMO and HOMO–2 → LUMO transitions. The HOMOs–1 and HOMOs–2 have higher Ir contribution (27–59%) than that in LUMOs (3–4%), whereas the LUMOs have higher N^N contribution (93%) than those in HOMOs–1 and HOMOs–2 (3–15%), therefore the transitions contain some Ir → π*(N^N) MLCT character. This finding is consistent with the spectroscopic observation that a red-shift in absorption energy is observed when N^N is changed from Me_2bpy to bpy, and from phen to dpq. Besides, the contribution of C^C^C to both the HOMOs–1 and HOMOs–2 are not low (27–69%), suggesting that the C^C^C ligands contribute significantly to the $d_\pi(Ir^{III})$ levels. The electronic difference density plots for **1a'** and **2a'** in their lowest-energy excited state (Figure 6, generated by taking the difference in the excited-state electron density and ground-state electron density) clearly show that electronic charge is depleted from the Ir center and accumulated at the N^N moiety. The emissions from complexes **1**–**2** are thus believed to be originated from the triplet $d_\pi(Ir^{III}) \rightarrow \pi^*$(N^N) MLCT states.

Conclusion

In this work a series of emissive Ir(III) hydrido complexes bearing the NHC-derived tridentate C^C^C pincer ligands and aromatic diimines have been prepared. This joint experimental and theoretical study reveals that the lowest-energy absorptions associated with these complexes arise from a $d_\pi(Ir^{III}) \rightarrow \pi^*$(N^N) MLCT transition, where the C^C^C ligands contribute significantly to the $d_\pi(Ir^{III})$ level. It is therefore evident that the C^C^C ligands can modulate the photophysical properties via the formation of the hybrid [Ir + C^C^C] molecular orbitals, and this work highlights the opportunities of using NHC-derived ligands to modulate the photophysics of a [M(N^N)] core.

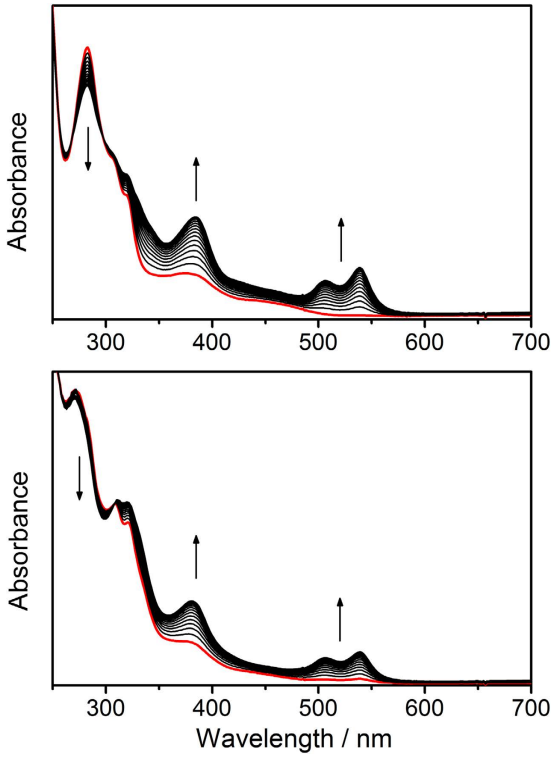

Figure 4. UV–visible absorption spectra for 1a (top) and 2a (bottom) in CH_3CN at 298 K during electrochemical reduction at −1.95 V vs $Cp_2Fe^{+/0}$ (10 s traces; initial trace is shown in red).

Methods

General Procedure. All reactions were performed under an argon atmosphere using standard Schlenk techniques unless otherwise stated. All reagents and solvents were used as received. The C^C^C ligand precursors, i.e. benzene-bridged bisimidazolium bromide[48], and $[Ir(1,5\text{-cod})Cl]_2$ (cod = 1,5-cyclooctadiene)[49], were prepared according to literature methods. [Ir(C^C^C)(CH_3CN)(Br)(H)] were synthesized analogously to the corresponding known complexes [Ir(^{Ar}C^C^C^{Ar})(CH_3CN)(Cl)(H)] and [Ir(^{Me}C^1^C^C^{1Me})(CH_3CN)(I)(H)][23,24]. ^{1}H, ^{13}C{^{1}H}, DEPT-135, ^{1}H–^{1}H COSY, and ^{1}H–^{13}C HSQC NMR spectra were recorded on Bruker 400 DRX FT-NMR spectrometer. Figure 7 depicts the labeling scheme for the H and C atoms. Peak positions were calibrated with solvent residue peaks as internal standard. Electrospray mass spectrometry was performed on a PE-SCIEX API 3000 triple quadrupole mass spectrometer. Infrared spectra were recorded as KBr plates on an Avatar 360 FTIR spectrometer. UV–visible spectra were recorded on a Shimadzu UV-1700 spectrophotometer. Elemental analyses were done on an Elementar Vario Micro Cube carbon–hydrogen–nitrogen elemental micro-analyzer. Cyclic voltammetry was performed with a CH Instrument model 600C series electrochemical analyzer/workstation. All the electrochemical measurements were performed in CH_3CN solution with [n-Bu_4N]PF_6 (0.1 M) as supporting electrolyte at room temperature. The glassy-carbon working electrode was polished with 0.05 μm alumina on a microcloth, sonicated for 5 min in deionized water, and rinsed with CH_3CN before use. An $Ag/AgNO_3$ (0.1 M in CH_3CN) electrode was used as reference electrode, with a platinum wire as the counter electrode. All solutions were degassed with nitrogen before experiments. The $E_{1/2}$ value of the ferrocenium/ferrocene couple ($Cp_2Fe^{+/0}$) measured in the same solution was used as an internal reference. Steady-state emission spectra were obtained on a Jobin Yvon Fluorolog-3-TCSPC spectrophotometer. Sample and standard solutions were degassed with at least three freeze-pump-thaw cycles. The emission quantum yields for complexes **1**–**2** were measured by the method of Demas and Crosby[50] with $[Ru(bpy)_3](PF_6)_2$ in degassed CH_3CN as standard ($\Phi_r = 0.062$), whereas that for $[Ir(C^1\text{^}C\text{^}C^1)_2]^+$ was measured with quinine sulphate in 0.1M H_2SO_4 as standard ($\Phi_r = 0.58$)[51]. The emission quantum yields were calculated by $\Phi_s = \Phi_r(B_r/B_s)(n_s/n_r)^2(D_s/D_r)$, where the subscripts s and r refer to sample and reference standard solution, respectively, n is the refractive index of the solvents, D is the integrated intensity, and Φ is the luminescence quantum yield. The quantity B is calculated by $B = 1 - 10^{-AL}$, where A is the absorbance at the excitation wavelength and L is the optical path length[52].

[Ir(C^C^C)(N^N)H](ClO_4), 1–2(ClO_4). A mixture of $[Ir(1,5\text{-cod})Cl]_2$ (0.10 mmol), benzene bridged bisimidazolium or bisbenzimidazolium bromide (0.20 mmol), and Cs_2CO_3 (0.43 mmol) was refluxed in CH_3CN (30 ml) for 16 h. Upon cooling to room temperature, the solvent was removed by reduced pressure and the residue was extracted with CH_2Cl_2. The [Ir(C^C^C)(CH_3CN)(Br)(H)] obtained from this

complex	λ_{em}/nm	Quantum yield (Φ)	Lifetime (τ)/ns
Solvent = CH_3CN			
1a	577	4.53×10^{-3}	21
1b	563	3.50×10^{-2}	244
1c	565	1.09×10^{-2}	38
1d	580	7.97×10^{-3}	30
2a	588	2.00×10^{-3}	10
2b	575	8.99×10^{-3}	51
2c	575	4.18×10^{-3}	15
2d	604	2.45×10^{-3}	11
$[Ir(C^1\text{^}C\text{^}C^1)_2]^+$	378	4.22×10^{-1} [b]	4663
	398		4802
	sh, 416		5001
Solvent = CH_2Cl_2			
1a	568	1.34×10^{-2}	47
1b	553	1.19×10^{-1}	790
1c	555	3.31×10^{-2}	91
1d	567	3.82×10^{-2}	121
2a	578	6.03×10^{-3}	26
2b	560	4.92×10^{-2}	181
2c	566	1.35×10^{-2}	43
2d	584	1.16×10^{-2}	51
$[Ir(C^1\text{^}C\text{^}C^1)_2]^+$	378	6.07×10^{-1} [b]	4906
	398		5094
	sh, 416		5298

Table 4. Emission Data for Complexes 1, 2, and $[Ir(C^1\text{^}C\text{^}C^1)_2]^+$ in solution at 298 K. Measurement conditions: Concentration = 3.0×10^{-5} M; λ_{ex} = 420 nm for **1–2**, 340 nm for $[Ir(C^1\text{^}C\text{^}C^1)_2]^+$. Quantum yields for complexes **1–2** and $[Ir(C^1\text{^}C\text{^}C^1)_2]^+$ were determined using $[Ru(bpy)_3]^{2+}$ and quinine sulphate as references, respectively.

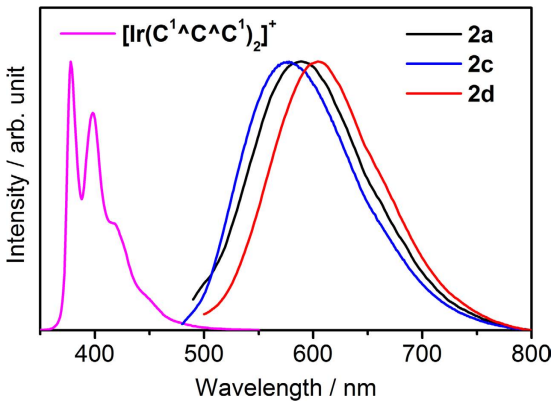

Figure 5. Emission spectra for 2a, 2c, 2d, and $[Ir(C^1\text{^}C\text{^}C^1)_2]^+$ (λ_{ex} = 420 nm for 1–2, 340 nm for $[Ir(C^1\text{^}C\text{^}C^1)_2]^+$).

extract was used for the synthesis of **1–2** without further purification. A mixture of [Ir(C^C^C)(CH_3CN)(Br)(H)] (0.15 mmol) and diimine (0.5 mmol) was refluxed in ethylene glycol for 3 h. Upon cooling to room temperature, the resultant solution was added to a saturated $NaClO_4$ solution to give brown solids. The crude product was eluted by column chromatography (neutral alumina, 9:1 (v/v) CH_2Cl_2/CH_3CN as

complex	experimental λ_{max}/cm^{-1} ($\varepsilon_{max}/dm^3\ mol^{-1}\ cm^{-1}$)	TD-DFT calculations	
		excitation energy/cm^{-1} (oscillator strength)	contribution
1a'	22780 (sh, 1620)	21540 (0.0086)	88.8% HOMO–1 → LUMO
			7.41% HOMO–2 → LUMO
			1.30% HOMO → LUMO
	26740 (4240)	25100 (0.1077)	87% HOMO–2 → LUMO
			7.07% HOMO–1 → LUMO
2a'	23700 (sh, 1710)	23260 (0.0121)	89.6% HOMO–1 → LUMO
			5.12% HOMO–2 → LUMO
			3.02% HOMO–3 → LUMO
			1.13% HOMO–8 → LUMO
	27030 (sh, 5240)	25920 (0.1109)	86.6% HOMO–2 → LUMO
			6.11% HOMO–1 → LUMO
			2.09% HOMO–3 → LUMO

Table 5. Calculated Vertical Transition Energies ($\lambda > 360$ nm) for 1a' and 2a' at the TD–DFT/COSMO level (Solvent = CH_3CN). Excitations with oscillator strength $< 5 \times 10^{-3}$ are omitted; solvent = CH_3CN.

complex	MO	% composition			
		Ir	N^N	C^C^C	$H_{hydride}$
1a'	HOMO–2	58.93	14.51	26.56	0.00
	HOMO–1	34.22	3.77	61.99	0.02
	HOMO	33.74	4.45	61.53	0.28
	LUMO	3.50	92.93	3.57	0.00
2a'	HOMO–3	10.46	1.13	88.41	0.00
	HOMO–2	56.27	13.54	30.19	0.00
	HOMO–1	27.45	3.35	69.20	0.01
	HOMO	27.81	3.80	68.07	0.32
	LUMO	3.41	92.87	3.72	0.00

Table 6. Selected Molecular Orbital Compositions (%) for 1a' and 2a'.

eluent) as a yellow band. After removal of solvent, the yellow solid was recrystallized by slow diffusion of Et_2O into CH_3CN solution to give yellow crystals.

Complex 1a. Yield: 0.06 g, 50%. Anal. Calcd for $C_{30}H_{34}N_6Ir(ClO_4)$: C, 46.78; H, 4.45; N, 10.91. Found: C, 46.70; H, 4.51; N, 10.88. ^{1}H NMR (400 MHz, CD_3CN): δ –20.46 (s, 1H, Ir−H), 0.58–0.99, 1.18–1.32 (m, 14H, C_3H_7 of *n*-Bu); 3.17–3.22 (m, 4H, CH_2 of *n*-Bu); 7.05 (d, 2H, $J = 2.1$ Hz, H_l); 7.16–7.16 (m, 1H, H_g); 7.22–7.29 (m, 3H, $H_i + H_j$); 7.41 (d, 1H, $J = 5.2$ Hz, H_h); 7.65–7.69 (m, 1H, H_b); 7.74 (d, 2H, $J = 2.1$ Hz, H_k); 7.88 (td, 1H, $J = 8.0$, 1.6 Hz, H_f); 8.21 (td, 1H, $J = 8.0$, 1.6 Hz, H_c); 8.38 (d, 1H, $J = 8.0$ Hz, H_e); 8.55 (d, 1H, $J = 8.0$ Hz, H_d); 9.67 (d, 1H, $J = 5.2$ Hz, H_a). ^{13}C NMR (100 MHz, CD_3CN): δ 13.7, 20.2, 34.5, 50.1 (*n*-Bu); 108.3 (C_j); 117.0 (C_k); 121.6 (C_l); 122.9 (C_i); 124.6 (C_e); 125.3 (C_d); 127.7 (C_g); 129.0 (C_b); 138.2 (C_c); 138.3 (C_f); 142.9 (Ir−C_{Ph}); 146.1 (Quaternary C in C^1^C^C^1); 151.7 (C_h); 156.9, 157.0 (Quaternary C in bpy); 157.2 (C_a); 167.9 (Ir−$C_{carbene}$). IR (KBr, cm^{-1}): $\nu_{Ir-H} = 2189$, $\nu_{Cl-O} = 1086$. ESI-MS: *m/z* 670 [M^+].

Complex 1b. Yield: 0.06 g, 50%. Anal. Calcd for $C_{32}H_{34}N_6Ir(ClO_4)$: C, 48.39; H, 4.31; N, 10.58. Found: C, 48.08; H, 4.36; N, 10.40. ^{1}H NMR (400 MHz, CD_3CN): δ –20.27 (s, 1H, Ir−H), 0.14–0.51, 0.89–1.06 (m, 14H, C_3H_7 of *n*-Bu); 2.92–3.15 (m, 4H, CH_2 of *n*-Bu); 6.98 (d, 2H, $J = 2.0$ Hz, H_l); 7.21–7.37 (m, 3H, $H_i + H_j$); 7.51 (dd, 1H, $J = 8.0$, 5.0 Hz, H_g); 7.74 (d, 2H, $J = 2.0$ Hz, H_k); 7.77 (d, 1H, $J = 5.0$ Hz, H_h); 8.04 (dd, 1H, $J = 8.0$, 5.0 Hz, H_b); 8.12 (d, 1H, $J = 8.8$ Hz, H_e); 8.22 (d, 1H, $J = 8.8$ Hz, H_d); 8.44 (d, 1H, $J = 8.0$ Hz, H_f); 8.78 (d, 1H, $J = 8.0$ Hz, H_c); 9.97 (d, 1H, $J = 5.0$ Hz, H_a). ^{13}C NMR (100 MHz, CD_3CN): δ 13.6, 20.0, 34.4, 50.1 (*n*-Bu); 108.4 (C_j); 117.1 (C_k); 121.6 (C_l); 123.2 (C_i); 126.4 (C_g); 127.8 (C_b); 128.8 (C_d); 128.9 (C_e); 132.1, 132.6 (Quaternary C in phen); 137.4 (C_c); 137.6 (C_f); 142.6 (Ir−C_{Ph});

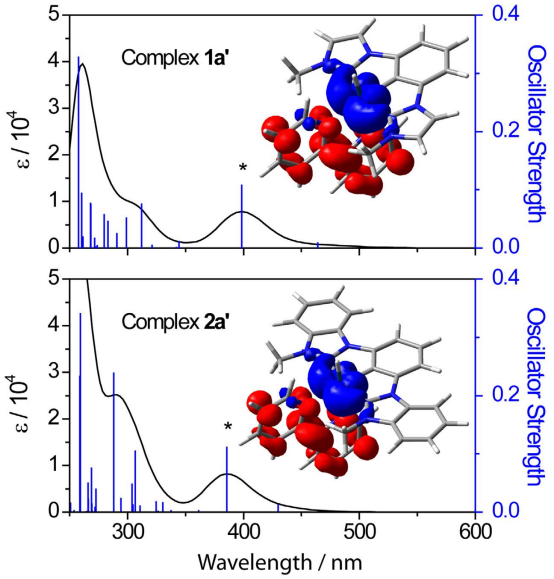

Figure 6. TD-DFT calculated absorption spectrum for model complexes 1a' and 2a' in CH_3CN. Excitation energies and oscillator strengths are shown by the blue vertical lines; spectrum (in black) is convoluted with a Gaussian function having a full width at half-maximum of 3000 cm^{-1}. Inserts show the electronic difference density plots for **1a'** and **2a'** at the vertical transitions marked with * (isodensity value = 0.002 au; charge accumulation and depletion are represented in red and blue respectively).

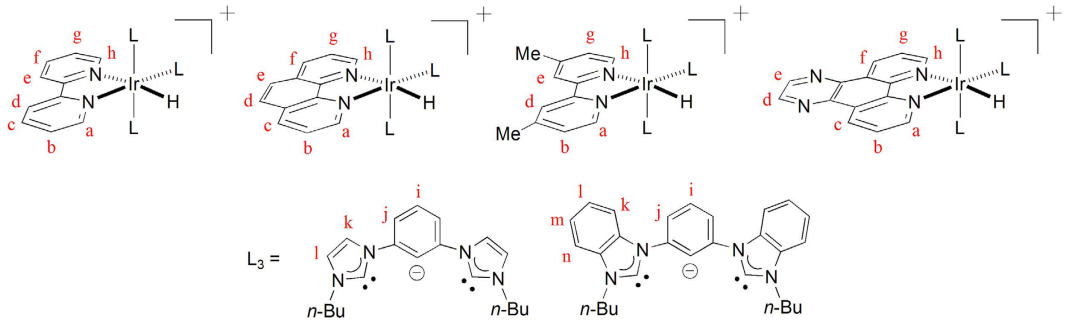

Figure 7. Labeling scheme for H and C atoms in 1–2.

146.4 (Quaternary C in C^1^C^C^1); 148.4, 148.8 (Quaternary C in phen); 152.6 (C_h); 157.3 (C_a); 168.1 (Ir−$C_{carbene}$). IR (KBr, cm^{-1}): ν_{Ir-H} = 2179, ν_{Cl-O} = 1094. ESI-MS: *m/z* 695 [M^+].

Complex 1c. Yield: 0.05 g, 40%. Anal. Calcd for $C_{32}H_{38}N_6Ir(ClO_4)$: C, 48.14; H, 4.80; N, 10.53. Found: C, 48.44; H, 5.08; N, 10.45. ^1H NMR (400 MHz, CD_3CN): δ −20.55 (s, 1H, Ir−H), 0.58–0.98, 1.19–1.38 (m, 14H, C_3H_7 of *n*-Bu); 2.39 (s, 3H, CH_3 of Me_2bpy); 2.61 (s, 3H, CH_3 of Me_2bpy); 3.26 (t, 4H, *J* = 7.8 Hz, CH_2 of *n*-Bu); 6.96 (d, 1H, *J* = 5.6 Hz, H_g); 7.05 (d, 2H, *J* = 2.1 Hz, H_l); 7.20 (d, 1H, *J* = 5.6 Hz, H_h); 7.21–7.29 (m, 3H, $H_i + H_j$); 7.50 (d, 1H, *J* = 5.6 Hz, H_b); 7.73 (d, 2H, *J* = 2.1 Hz, H_k); 8.23 (s, 1H, H_e); 8.39 (s, 1H, H_d); 9.46 (d, 1H, *J* = 5.6 Hz, H_a). ^{13}C NMR (100 MHz, CD_3CN): δ 13.7, 20.3, 34.5, 50.1 (*n*-Bu); 21.1, 21.3 (CH_3 of Me_2bpy); 108.2 (C_j); 117.0 (C_k); 121.5 (C_l); 122.7 (C_i); 125.2 (C_e); 125.8 (C_d); 128.4 (C_g); 129.6 (C_b); 143.4 (Ir−C_{Ph}); 146.1 (Quaternary C in C^1^C^C^1); 150.5, 150.7 (Quaternary C in Me_2bpy); 150.9 (C_h); 156.6 (C_a); 156.8, 156.9 (Quaternary C in Me_2bpy); 168.4 (Ir−$C_{carbene}$). IR (KBr, cm^{-1}): ν_{Ir-H} = 2159, ν_{Cl-O} = 1107. ESI-MS: *m/z* 699 [M^+].

Complex 1d. Yield: 0.06 g, 45%. Anal. Calcd for $C_{34}H_{34}N_8Ir(ClO_4)$: C, 48.25; H, 4.05; N, 13.24. Found: C, 48.47; H, 4.28; N, 13.06. ^1H NMR (400 MHz, CD_3CN): δ −20.29 (s, 1H, Ir−H), 0.27–0.75, 1.08–1.21 (m, 14H, C_3H_7 of *n*-Bu); 2.91–3.22 (m, 4H, CH_2 of *n*-Bu); 7.00 (d, 2H, *J* = 2.1 Hz, H_l); 7.24–7.37 (m, 3H, $H_i + H_j$); 7.65 (dd, 1H, *J* = 8.2, 5.2 Hz, H_g); 7.76 (d, 2H, *J* = 2.0 Hz, H_k); 7.87–7.88 (m, 1H, H_h); 8.18 (dd, 1H, *J* = 8.2, 5.2 Hz, H_b); 9.18 (d, 1H, *J* = 2.1 Hz, H_e); 9.22 (d, 1H, *J* = 2.1 Hz, H_d); 9.41 (dd, 1H, *J* = 8.2, 1.2 Hz, H_f); 9.75 (dd, 1H, *J* = 8.2, 1.2 Hz, H_c); 10.09 (dd, 1H, *J* = 5.2, 1.2 Hz, H_a). ^{13}C NMR (100 MHz, CD_3CN): δ 13.5, 20.1, 34.3, 50.2 (*n*-Bu); 108.5 (C_j); 117.2 (C_k); 121.7 (C_l); 123.3 (C_i); 127.6 (C_g); 128.9

(C_b); 130.8, 131.5 (Quaternary C in dpq); 134.0 (C_c); 134.2 (C_f); 140.5, 140.5 (Quaternary C in dpq); 142.2 (Ir−C_{Ph}); 146.3 (Quaternary C in C^1^C^C^1); 147.7, 147.8 (C_d + C_e); 149.7, 150.0 (Quaternary C in dpq); 153.9 (C_h); 158.5 (C_a); 167.8 (Ir−$C_{carbene}$). IR (KBr, cm^{-1}): ν_{Ir-H} =2131, ν_{Cl-O} = 1108. ESI-MS: *m/z* 747 [M$^+$].

Complex 2a. Yield: 0.07 g, 50%. Anal. Calcd for $C_{38}H_{38}N_6Ir(ClO_4)$: C, 52.44; H, 4.40; N, 9.66. Found: C, 52.45; H, 4.38; N, 9.46. ^{1}H NMR (400 MHz, CD_3CN): δ –19.50 (s, 1H, Ir−H), 0.40–1.07, 1.23–1.47 (m, 14H, C_3H_7 of *n*-Bu); 3.30–3.59 (m, 4H, CH_2 of *n*-Bu); 7.07 (t, 1H, J = 6.4 Hz, H_g); 7.28–7.35 (m, 2H, H_m); 7.37–7.50 (m, 6H, H_h + H_i + H_l + H_n); 7.71–7.74 (m, 1H, H_b); 7.77–7.87 (m, 3H, H_j + H_f); 8.21 (d, 2H, J = 8.0 Hz, H_k); 8.27–8.31 (m, 1H, H_c); 8.38 (d, 1H, J = 8.2 Hz, H_e); 8.60 (d, 1H, J = 8.2 Hz, H_d); 9.51 (d, 1H, J = 5.3 Hz, H_a). ^{13}C NMR (100 MHz, CD_3CN): δ 13.8, 20.4, 33.3, 47.5 (*n*-Bu); 109.7 (C_j); 111.9 (C_l/C_n); 112.2 (C_k); 123.6 (C_i); 123.9 (C_m); 124.6 (C_e); 124.7 (C_l/C_n); 125.5 (C_d); 127.9 (C_g); 129.3 (C_b); 133.0, 135.6 (Quaternary C in C^2^C^C^2); 138.7 (C_f); 138.8 (C_c); 142.9 (Ir−C_{Ph}); 146.6 (Quaternary C in C^2^C^C^2); 152.2 (C_h); 156.6 (Quaternary C in bpy); 157.2 (C_a); 157.3 (Quaternary C in bpy); 180.1 (Ir−$C_{carbene}$). IR (KBr, cm^{-1}): ν_{Ir-H} = 2126, ν_{Cl-O} = 1075 ESI-MS: *m/z* 771 [M$^+$].

Complex 2b. Yield: 0.05 g, 40%. Anal. Calcd for $C_{40}H_{38}N_6Ir(ClO_4)$: C, 53.71; H, 4.28; N, 9.40. Found: C, 53.75; H, 4.30; N, 9.45. ^{1}H NMR (400 MHz, CD_3CN): δ –19.21 (s, 1H, Ir−H), 0.19–0.35, 0.38–0.45, 0.52–0.67 (m, 14H, C_3H_7 of *n*-Bu); 3.26–3.46 (m, 4H, CH_2 of *n*-Bu); 7.26–7.39 (m, 4H, H_l/H_m + H_n); 7.39–7.48 (m, 3H, H_g + H_m/H_l); 7.52 (t, 1H, J = 8.0 Hz, H_i); 7.81 (d, 2H, J = 5.1 Hz, H_f); 7.87 (d, 2H, J = 8.0 Hz, H_j); 8.08–8.18 (m, 2H, H_b + H_e); 8.21–8.29 (m, 3H, H_d + H_k); 8.41 (d, 1H, J = 8.2 Hz, H_h); 8.88 (d, 1H, J = 8.2 Hz, H_c); 9.96 (d, 1H, J = 8.2 Hz, H_a). ^{13}C NMR (100 MHz, CD_3CN): δ 13.8, 20.3, 33.3, 47.6 (*n*-Bu); 109.8 (C_j); 111.9 (C_l/C_m/C_n); 112.3 (C_k); 123.9 (C_i); 124.0 (C_l/C_m/C_n); 124.8 (C_l/C_m/C_n); 126.7 (C_g); 128.1 (C_b); 128.8 (C_d); 129.1 (C_e); 132.2, 132.7 (Quaternary C in phen); 133.1, 135.7 (Quaternary C in C^2^C^C^2); 137.9 (C_h); 138.1 (C_c); 142.6 (Ir−C_{Ph}); 146.9 (Quaternary C in C^2^C^C^2); 148.3, 148.9 (Quaternary C in phen); 153.2 (C_f); 157.4 (C_a); 180.4 (Ir−$C_{carbene}$). IR (KBr, cm^{-1}): ν_{Ir-H} = 2129, ν_{Cl-O} = 1090. ESI-MS: *m/z* 795 [M$^+$].

Complex 2c. Yield: 0.05 g, 40%. Anal. Calcd for $C_{40}H_{42}N_6Ir(ClO_4)$: C, 53.47; H, 4.71; N, 9.35. Found: C, 53.53; H, 4.77; N, 9.57. ^{1}H NMR (400 MHz, CD_3CN): δ –19.48 (s, 1H, Ir−H), 0.60–0.97, 1.34–1.47 (m, 14H, C_3H_7 of *n*-Bu); 2.33 (s, 3H, CH_3 of Me_2bpy); 2.67 (s, 3H, CH_3 of Me_2bpy); 3.39–3.67 (m, 4H, CH_2 of *n*-Bu); 6.90 (d, 1H, J = 5.7 Hz, H_g); 7.25 (d, 1H, J = 5.7 Hz, H_h); 7.28–7.38 (m, 2H, H_m); 7.40–7.50 (m, 5H, H_i + H_l + H_n); 7.54–7.65 (m, 1H, H_b); 7.81 (d, 2H, J = 8.0 Hz, H_j); 8.17–8.35 (m, 3H, H_e + H_k); 8.46 (s, 1H, H_d); 9.42 (d, 1H, J = 5.6 Hz, H_a). ^{13}C NMR (100 MHz, CD_3CN): δ 13.8, 20.5, 33.4, 47.6 (*n*-Bu); 21.1, 21.3 (CH_3 of Me_2bpy); 109.6 (C_j); 111.9 (C_l/C_n); 112.2 (C_k); 123.5 (C_i); 123.9 (C_m); 124.7 (C_l/C_n); 125.3 (C_e); 126.0 (C_d); 128.6 (C_g); 130.0 (C_b); 133.0, 135.7 (Quaternary C in C^2^C^C^2); 143.4 (Ir−C_{Ph}); 146.7 (Quaternary C in C^2^C^C^2); 151.1, 151.3 (Quaternary C in Me_2bpy); 151.3 (C_h); 156.6 (Quaternary C in Me_2bpy); 156.7 (C_a); 157.1 (Quaternary C in Me_2bpy); 180.6 (Ir−$C_{carbene}$). IR (KBr, cm^{-1}): ν_{Ir-H} = 2133, ν_{Cl-O} = 1094. ESI-MS: *m/z* 799 [M$^+$].

Complex 2d. Yield: 0.06 g, 40%. Anal. Calcd for $C_{42}H_{38}N_8Ir(ClO_4)$: C, 53.30; H, 4.05; N, 11.84. Found: C, 53.41; H, 4.25; N, 11.94. ^{1}H NMR (400 MHz, CD_3CN): δ –19.22 (s, 1H, Ir−H), 0.23–0.79, 1.18–1.48 (m, 14H, C_3H_7 of *n*-Bu); 3.17–3.61 (m, 4H, CH_2 of *n*-Bu); 7.28–7.46 (m, 6H, H_l + H_m + H_n); 7.54 (t, 1H, J = 8.0 Hz, H_i); 7.59 (dd, 1H, J = 8.2, 5.2 Hz, H_g); 7.89 (d, 2H, J = 8.0 Hz, H_j); 7.91–7.93 (m, 1H, H_h); 8.16–8.35 (m, 3H, H_b + H_k); 9.18 (d, 1H, J = 2.1 Hz, H_e); 9.24 (d, 1H, J = 2.1 Hz, H_d); 9.37 (dd, 1H, J = 8.2, 1.4 Hz, H_f); 9.85 (dd, 1H, J = 8.2, 1.3 Hz, H_c); 10.11 (dd, 1H, J = 5.2, 1.3 Hz, H_a). ^{13}C NMR (100 MHz, CD_3CN): δ 13.7, 20.4, 33.3, 47.7 (*n*-Bu); 109.9 (C_j), 112.0 (C_l/C_m/C_n); 112.3 (C_k); 124.1 (C_i); 124.1, 124.9 (C_l/C_m/C_n); 127.8 (C_g); 129.2 (C_b); 130.9, 131.6 (Quaternary C in dpq); 133.1 (Quaternary C in C^2^C^C^2); 134.5 (C_c), 134.6 (C_f), 135.7 (Quaternary C in C^2^C^C^2); 140.4, 140.5 (Quaternary C in dpq); 142.3 (Ir−C_{Ph}), 146.9 (Quaternary C in C^2^C^C^2), 147.8 (C_e); 147.9 (C_d); 149.5, 150.2 (Quaternary C in dpq); 154.5 (C_h); 158.6 (C_a); 180.1 (Ir−$C_{carbene}$). IR (KBr, cm^{-1}): ν_{Ir-H} = 2130, ν_{Cl-O} = 1097. ESI-MS: *m/z* 847 [M$^+$].

X-ray Crystallography. X-ray diffraction data for **1a**(ClO_4), **2a**(ClO_4), and [**2b**(ClO_4)]$_3$·CH_3CN were collected on an Oxford Diffraction Gemini S Ultra X-ray single crystal diffractometer with Cu Kα radiation (λ = 1.54178 Å) at 133 K. The data were processed using CrysAlis[53]. The structures were solved by Patterson and Fourier methods and refined by full-matrix least-squares based on F^2 with program SHELXS-97 and SHELXL-97[54] within WinGX[55]. All non-hydrogen atoms were refined anisotropically in the final stage of least-squares refinement. The positions of H atoms were calculated based on riding mode with thermal parameters equal to 1.2 times that of the associated C atoms. CCDC 1416088–1416090 contain the supplementary crystallographic data for this paper, which can be obtained free of charge from The Cambridge Crystallographic Data Centre via www.ccdc.cam.ac.uk/data_request/cif.

Computational Methodology. DFT calculations were performed on model complexes [Ir(^{Me}C^1^C^C^{1Me})(bpy)(H)]$^+$ (**1a'**) and [Ir(^{Me}C^2^C^C^{2Me})(bpy)(H)]$^+$ (**2a'**). Their electronic ground states

were optimized without symmetry constrain using the density functional PBE0[45,46]. The def2-SVP basis sets were used for the H, C, and N atoms, while the def2-TZVP(-f) basis sets were used for the Ir atoms[56]. Zero-order regular approximation (ZORA) was employed to account for relativistic effects. Tight SCF convergence (10^{-8}au) was used for all calculations. The vertical transition energies for these model complexes in CH_3CN were computed at their respective gas-phase optimized ground-state geometries using time-dependent-DFT (TD-DFT) method with the same density functional and basis sets in the geometry optimizations. The combination of the resolution of the identity and the "chain of spheres exchange" algorithms (RIJCOSX)[57] was used to accelerate all DFT and TD-DFT calculations with the use of appropriate auxiliary basis sets. The conductor-like screening model (COSMO)[47] was used to account for solvent effects upon the electronic transition. All the calculations were performed using the ORCA software package (version 3.0.2)[58].

References

1. Kalyanasundaram, K. Photophysics, Photochemistry and Solar Energy Conversion with Tris(bipyridyl)ruthenium(II) and its Analogues. *Coord. Chem. Rev.* **46,** 159–244 (1982).
2. Balzani, V., Sabbatini, N. & Scandola, F. "Second-sphere" Photochemistry and Photophysics of Coordination Compounds. *Chem. Rev.* **86,** 319–337 (1986).
3. Juris, A. *et al.* Ru(II) Polypyridine Complexes: Photophysics, Photochemistry, Electrochemistry, and Chemiluminescence. *Coord. Chem. Rev.* **84,** 85–277 (1988).
4. Meyer, T. J. Chemical Approaches to Artificial Photosynthesis. *Acc. Chem. Res.* **22,** 163–170 (1989).
5. Balzani, V., Barigelletti, F. & De Cola, L. Metal Complexes as Light Absorption and Light Emission Sensitizers. *Top. Curr. Chem.* **158,** 31–71 (1990).
6. Sauvage, J.-P. *et al.* Ru(II) and Osmium(II) Bis(terpyridine) Complexes in Covalently-Linked Multicomponent Systems: Synthesis, Electrochemical Behavior, Absorption Spectra, and Photochemical and Photophysical Properties. *Chem. Rev.* **94,** 993–1019 (1994).
7. Balzani, V. *et al.* Luminescent and Redox-Active Polynuclear Transition Metal Complexes. *Chem. Rev.* **96,** 759–833 (1996).
8. De Silva, A. P. *et al.* Signaling Recognition Events with Fluorescent Sensors and Switches. *Chem. Rev.* **97,** 1515–1566 (1997).
9. Dixon, I. M. *et al.* A Family of Luminescent Coordination Compounds: Iridium(III) Polyimine Complexes. *Chem. Soc. Rev.* **29,** 385–391 (2000).
10. De Cola, L. *et al.* Design, Synthesis and Photophysics of Ruthenium and Osmium Complexes through 20 Years of Collaboration. *Inorg. Chim. Acta.* **360,** 775–784 (2007).
11. Campagna, S. *et al.* Photochemistry and Photophysics of Coordination Compounds: Ruthenium. *Top. Curr. Chem.* **280,** 117–214 (2007).
12. Flamigni, L. *et al.* Photochemistry and Photophysics of Coordination Compounds: Iridium. *Top. Curr. Chem.* **281,** 143–203 (2007).
13. Flamigni, L., Collin, J.-P. & Sauvage, J.-P. Iridium Terpyridine Complexes as Functional Assembling Units in Arrays for the Conversion of Light Energy. *Acc. Chem. Res.* **41,** 857–871 (2008).
14. Lainé, P. P., Campagna, S. & Loiseau, F. Conformationally Gated Photoinduced Processes within Photosensitizer-Acceptor Dyads Based on Ruthenium(II) and Osmium(II) Polypyridyl Complexes with an Appended Pyridinium Group. *Coord. Chem. Rev.* **252,** 2552–2571 (2008).
15. Balzani. V. & Juris, A. Photochemistry and Photophysics of Ru(II)-Polypyridine Complexes in the Bologna Group. From Early Studies to Recent Developments. *Coord. Chem. Rev.* **211,** 97–115 (2001).
16. Chou, P.-T. & Chi, Y. Phosphorescent Dyes for Organic Light-Emitting Diodes. *Chem. Eur. J.* **13,** 380–395 (2007).
17. Erkkila, K. E., Odom, D. T. & Barton, J. K. Recognition and Reaction of Metallointercalators with DNA. *Chem. Rev.* **99,** 2777–2795 (1999).
18. Sajoto, T. *et al.* Blue and Near-UV Phosphorescence from Iridium Complexes with Cyclometalated Pyrazolyl or N-Heterocyclic Carbene Ligands. *Inorg. Chem.* **44,** 7992–8003 (2005).
19. Chang, C.-F.*et al.* Highly Efficient Blue-Emitting Iridium(III) Carbene Complexes and Phosphorescent OLEDs. *Angew. Chem. Int. Ed.* **47,** 4542–4545 (2008).
20. Arduengo, A. J., Harlow, R. L. & Kline, M. A Stable Crystalline Carbene. *J. Am. Chem. Soc.* **113,** 361–363 (1991).
21. Herrmann, W. A. N-Heterocyclic Carbenes: A New Concept in Organometallic Catalysis. *Angew. Chem. Int. Ed.* **41,** 1290–1309 (2002).
22. Clavier, H. & Nolan, S. P. Percent Buried Volume For Phosphine and N-Heterocyclic Carbene Ligands: Steric Properties in Organometallic Chemistry. *Chem. Commun.* **46,** 841–861 (2010).
23. Raynal, M. *et al.* An Unprecedented, Figure-Of-Eight, Dinuclear Iridium(I) Dicarbene and New Iridium(III) 'Pincer' Complexes. *Chem. Commun.* 3983–3985 (2008).
24. Raynal, M. *et al.* Reaction Intermediates in the Synthesis of New Hydrido, N-Heterocyclic Dicarbene Iridium(III) Pincer Complexes. *Organometallics* **28,** 4028–4047 (2009).
25. Chianese, A. R. *et al.* Iridium Complexes of CCC-Pincer N-Heterocyclic Carbene Ligands: Synthesis and Catalytic C-H Functionalization. *Organometallics*, **29,** 3019–3026 (2010).
26. Son, S. U. *et al.* Synthesis of Ru(II) Complexes of N-Heterocyclic Carbenes and Their Promising Photoluminescence Properties in Water. *Inorg. Chem.* **43,** 6896–6898 (2004).
27. Unger, Y. *et al.* Green–Blue Emitters: NHC-Based Cyclometalated [Pt(C^C*)(acac)] Complexes. *Angew. Chem. Int. Ed.* **49,** 10214–10216 (2010).
28. Barnard, P. J. *et al.* Luminescence Studies of The Intracellular Distribution of a Dinuclear Gold(I) N-Heterocyclic Carbene Complex. *Angew. Chem. Int. Ed.* **45,** 5966–5970 (2006).
29. Strasser, C. E. & Catalano, V. J. "On-off" Au(I)···Cu(I) Interactions in a $Au(NHC)_2$ Luminescent Vapochromic Sensor. *J. Am. Chem. Soc.* **132,** 10009–10011 (2010).
30. Chung, L.-H. *et al.* Emissive Osmium(II) Complexes Supported by N-Heterocyclic Carbene-based C^C^C-Pincer Ligands and Aromatic Diimines. *Inorg. Chem.* **51,** 8693–8703 (2012).
31. Chung, L.-H. *et al.* Ruthenium(II) and Osmium(II) Complexes Bearing Bipyridine and the N-Heterocyclic Carbene-Based C^N^C Pincer Ligand: An Experimental and Density Functional Theory Study. *Inorg. Chem.* **52,** 9885–9896 (2013).
32. Chung, L.-H. *et al.* Metal–Indolizine Zwitterion Complexes as a New Class of Organometallic Material: A Spectroscopic and Theoretical Investigation. *Organometallics* **33,** 3443–3452 (2014).
33. Tsui, W.-K. *et al.* Luminescent Ruthenium(II) Complex Bearing Bipyridine and N-Heterocyclic Carbene-based C^N^C Pincer Ligand for Live-Cell Imaging of Endocytosis. *Sci. Rep.* **5,** 9070 (2014).

34. Darensbourg, M. Y., Ludwig, M. & Riordan, C. G. Spectroscopic and Chemical Studies of Nickel(II) Hydrides. *Inorg. Chem.* **28,** 1630–1634 (1989).
35. Huynh, H. V. *et al.* ^{13}C NMR Spectroscopic Determination of Ligand Donor Strengths Using N-Heterocyclic Carbene Complexes of Palladium(II). *Organometallics* **28,** 5395–5404 (2009).
36. Cho, J. *et al.* An Improved Method for The Synthesis of Zirconium (CCC-N-Heterocyclic Carbene) Pincer Complexes and Applications in Hydroamination. *Chem. Commun.* 5001–5003 (2008).
37. Flynn, C. M. & Demas, J. N. Synthesis and Luminescence of the Tris(2,2'-Bipyridine)Iridium(III) Ion. *J. Am. Chem. Soc.* **96,** 1959–1960 (1974).
38. Ayala, N. P. *et al.* Synthesis, Luminescence, and Excited-State Complexes of the Tris(1,10-Phenanthroline)- and Bis(Terpyridine)-Iridium(III) Cations. *J. Am. Chem. Soc.* **112,** 3837–3844 (1990).
39. Wunschel, K. R. & Ohnesorge, W. E. Luminescence of iridium(III) chelates with 2,2'-bipyridine and with 1,10-phenanthroline. *J. Am. Chem. Soc.* **89,** 2777–2778 (1967).
40. Garces, F. O., King, K. A. & Watts, R. J. Synthesis, Structure, Electrochemistry, and Photophysics of Methyl-Substituted Phenylpyridine Ortho-Metalated Iridium(III) Complexes. *Inorg. Chem.* **27,** 3464–3471 (1988).
41. King, K. A. & Watts, R. J. Dual Emission from an Ortho-Metalated Ir(III) Complex. *J. Am. Chem. Soc.* **1987,** *109*, 1589–1590 (1987).
42. Ohsawa, Y. *et al.* Electrochemistry and Spectroscopy of Ortho-Metalated Complexes of Ir(III) and Rh(III). *J. Phys. Chem.* **91,** 1047–1054 (1987).
43. Ichimura, K. *et al.* Excited-state Absorption Spectroscopy of Ortho-Metalated Ir(III) Complexes. *J. Phys. Chem.* **91,** 6104–6106 (1987).
44. Coombe, V. T. *et al.* Spectroelectrochemical Studies on Tris(Bipyridyl)Iridium Complexes: Ultraviolet, Visible and Near-Infrared Spectra of the Series $[Ir(bpy)_3]^{3+/2+/+/0}$. *Inorg. Chem.* **23,** 3423–3425 (1984).
45. Perdew, J. P., Burke, K. & Ernzerhof, M. Generalized Gradient Approximation Made Simple. *Phys. Rev. Lett.* **77,** 3865–3868 (1996).
46. Adamo, C. & Barone, V. Toward reliable density functional methods without adjustable parameters: the PBE0 model. *J. Chem. Phys.* **110,** 6158–6170 (1999).
47. Klamt, A. & Schüürmann, G. COSMO: a new approach to dielectric screening in solvents with explicit expressions for the screening energy and its gradient. *J. Chem. Soc., Perkin Trans.* **2,** 799–805 (1993).
48. Vargas, V. C. *et al.* Efficient Route to 1,3-Di-N-imidazolylbenzene. A Comparison of Monodentate vs. Bidentate Carbenes in Pd-Catalyzed Cross Coupling. *Org. Lett.* **5,** 4847–4849 (2003).
49. Komiya, S. *Synthesis of Organometallic Compounds: A Practical Guide* (ed. Komiya, S.) (John Wiley and Sons Ltd, 1997).
50. Demas, J. N. & Crosby, G. A. The Measurement of Photoluminescence Quantum Yields. A Review. *J. Phys. Chem.* **75,** 991–1024 (1971).
51. Brouwer, A. M. Standards for Photoluminescence Quantum Yield Measurements in Solution (IUPAC Technical Reports). *Pure Appl. Chem.* **83,** 2213–2228 (2011).
52. Lakowicz, J. R. *Principles of Fluorescence Spectroscopy,* 2nd edn. (Kluwer Academic/Plenum Publishers, 1999).
53. CrysAlis, version 1.171.31.8; Oxford Diffraction Ltd.: Oxford, UK (2007).
54. Sheldrick, G. M. SHELXS-97 and SHELXL-97, *Program for Crystal Structure Solution and Refinements*; University of Göttingen: Göttingen, Germany (1997).
55. Farrugia, L. J. WinGX. *J. Appl. Crystallogr.* **32,** 837–838 (1999).
56. Weigend, F. & Ahlrichs, R. Balanced basis sets of split valence, triple zeta valence and quadruple zeta valence quality for H to Rn: Design and assessment of accuracy. *Phys. Chem. Chem. Phys.* **7,** 3297–3305 (2005).
57. Neese, F. An improvement of the resolution of the identity approximation for the formation of the Coulomb matrix. *J. Comput. Chem.* **24,** 1740–1747 (2003).
58. Neese, F. The ORCA program system. *WIREs Comput. Mol. Sci.* **2,** 73–78 (2012).

Acknowledgements

The work described in this paper was supported by the Hong Kong Research Grants Council (Project No. CityU 103911), and the Special Equipment Grant from the Hong Kong University Grants Committee (SEG_CityU02). We are grateful to Dr. Shek-Man Yiu for X-ray diffraction data collection and Mr. Pak-Kei Pat for technical support.

Author Contributions

L.H.C, H.S.L. and S.W.N. carried out all the experiments and performed the data analysis; D.L.M., C.H.L. and C.Y.W. designed the experiments, analyzed the results and wrote the manuscript. All authors reviewed the manuscript.

Additional Information

Competing financial interests: The authors declare no competing financial interests.

How to cite this article: Chung, L.-H. *et al.* Luminescent Iridium(III) Complexes Supported by N-Heterocyclic Carbene-based C^C^C-Pincer Ligands and Aromatic Diimines. *Sci. Rep.* **5**, 15394; doi: 10.1038/srep15394 (2015).